PCCP

Containerless solidification of undercooled $SrO–Al_2O_3$ binary melts

Journal:	*Physical Chemistry Chemical Physics*
Manuscript ID:	CP-ART-12-2014-005861.R2
Article Type:	Paper
Date Submitted by the Author:	29-Jan-2015

Complete List of Authors:	Kato, Katsuyoshi; The University of Tokyo, Institute of Industrial Science Masuno, Atsunobu; The University of Tokyo, Institute of Industrial Science Inoue, Hiroyuki; The University of Tokyo, Institute of Industrial Science

Journal Name

RSCPublishing

ARTICLE

Containerless solidification of undercooled SrO–Al_2O_3 binary melts

Cite this: DOI: 10.1039/x0xx00000x

Katsuyoshi Kato, Atsunobu Masuno,* and Hiroyuki Inoue

Received 00th January 2012,
Accepted 00th January 2012

DOI: 10.1039/x0xx00000x

www.rsc.org/

The solidification of the SrO–Al_2O_3 binary system was investigated under containerless conditions using an aerodynamic levitation furnace. Glass formation was observed in compositions with 35–45 mol% SrO and 55–75 mol% SrO. Cooling curves were obtained at a constant cooling rate in the range 1–1000°C/s. The crystallization temperature was apparently independent of the cooling rate and far below the melting point when the sample was fully crystallized, whereas it decreased when the sample was partially crystallized. The difference between the crystallization temperature and melting point under containerless conditions is considered a good measure of the glass-forming ability when there is not much difference in the critical cooling rates between the melt compositions. Furthermore, the homogeneous nucleation theory suggests that the apparent time-independent crystallization temperature is attributed to the high glass-forming ability of the SrO–Al_2O_3 binary system. The results suggest that the experimentally obtained continuous cooling transformation diagrams under containerless conditions provide new insights regarding solidification from an undercooled melt.

1. Introduction

When a melt is cooled, glass formation and crystallization compete. Crystallization is suppressed with an increasing cooling rate, and glass often forms at high cooling rates. The critical cooling rate R_C is defined as the lowest cooling rate at which a melt transforms to glass. R_C is regarded as a measure of the glass-forming ability of a melt. Good glass formers such as SiO_2 have very small R_C (~2×10^{-4}°C/s),[1] whereas R_C is over 10^5°C/s in oxides with low glass-forming ability such as Al_2O_3.[2] Time-temperature-transformation (TTT) and continuous cooling transformation (CCT) diagrams are used to evaluate the tendency for glass formation or crystallization and to estimate R_C.[1,3–13] A TTT diagram is constructed by measuring the time of crystallization at a given temperature, while a CCT diagram is constructed by measuring the temperature and time of crystallization at a given cooling rate. TTT or CCT diagrams are typically obtained using thermal analysis methods such as differential thermal analysis and differential scanning calorimetry.

Theoretical calculations were performed to construct TTT or CCT diagrams.[1,3–6,9,12] TTT diagrams are constructed using the time-independent homogeneous nucleation frequency and the rate of crystal growth. The glass-forming ability is quantitatively evaluated using calculated TTT diagrams; however, because theoretical calculations require thermophysical data such as temperature dependence of viscosity, which are often difficult to obtain, there are large discrepancies between theoretical calculations and experimental results. Furthermore, the effect of extrinsic heterogeneous nucleation, which occurs at the boundary between the melt and the wall of a container, should be considered.

In containerless processing, a melt is levitated without any contact; therefore, containerless processing provides an ideal platform for studying TTT and CCT diagrams under conditions where heterogeneous nucleation is suppressed. In addition, there is no contamination to cause crystallization, and extremely high temperatures (>2000°C) are easily reached via laser heating. Solidification of metallic alloys and oxides under containerless conditions have been investigated using levitation furnaces.[10,11,14–20]

SrO–Al_2O_3 binary compounds are always crystallized when using conventional melt-quenching techniques, indicating low glass-forming ability. However, some compositions do vitrify under containerless conditions because of the crystallization suppression,[21] meaning that the glass-forming ability depends greatly on chemical composition. In this binary system, the changes in glass-forming ability can be detected through CCT diagrams although the compositional range is narrow. In this study, we obtained CCT diagrams of SrO–Al_2O_3 binary compounds to evaluate the glass-forming ability under containerless conditions using an aerodynamic levitation (ADL) furnace. Furthermore, the containerless solidification was investigated on the basis of the homogeneous nucleation theory.

2. Experimental Procedure

$SrCO_3$ and α-Al_2O_3 powders were mixed (xSrO–(100−x)Al_2O_3, $0 \le x \le 80$), pressed into rods at 25 MPa, and sintered at 1100°C for 12 h in air. A bulk ceramic target weighing approximately 15 mg was taken from the rods and placed on the nozzle of an ADL furnace. The target was levitated by an O_2 gas flow and heated by two 100 W CO_2 lasers. The laser's incident angle is approximately 70°, and the two lasers were placed at opposite sides. The laser power was controlled by steps of 0.5%. The flow rate of the O_2 gas was controlled to maintain stable levitation of the melt using a mass flow controller.

The melt temperature was measured with a monochrome pyrometer (KLEIBER, KMGA 740-LO) at 100 kHz. The pyrometer spot size was always smaller than the melt size whose diameter was approximately 2 mm. The sample's emissivity is required to calculate the temperature from the pyrometer's signal. The emissivity was determined using the cooling curve of the melt. When the melt is cooled by turning off the laser, the melt temperature drops below the melting point, and it increases rapidly to the melting point because of the release of the latent heat when crystallization begins, which is called as recalescence. The temperature does not change at the melting point as long as the melt coexists with crystals. After the sample has fully crystallized, the temperature starts to decrease. The sample's emissivity is determined such that the plateau temperature is the same as the melting point reported in the literature. Figure 1 shows the enlarged view of the cooling curve of 35SrO–65Al_2O_3. Recalescence, which accompanies crystallization, and the plateau temperature are clearly observed. The emissivity of 35SrO–65Al_2O_3 was determined such that the plateau temperature is the same as the melting point, i.e., 1770°C.[22]

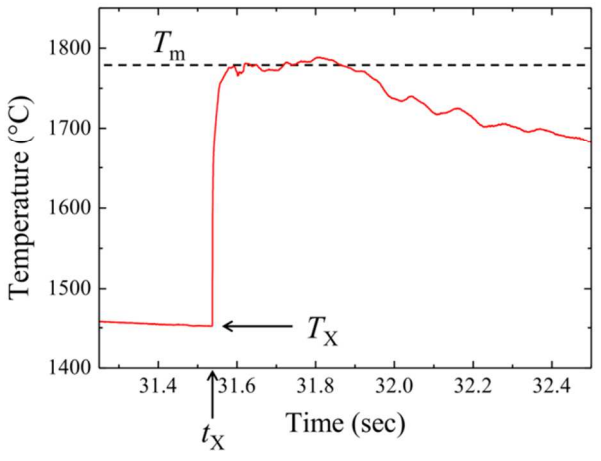

Fig. 1 Enlarged view of the cooling curve of 35SrO–65Al_2O_3. The crystallization time t_X and crystallization temperature T_X are the time and temperature at which recalescence accompanied with crystallization from melt starts. T_m is the melting point.

After determining the sample's emissivity, the solidification process was investigated. Before cooling, the melt was maintained at 2000°C, which is much higher than the melting point. The melt was then cooled to room temperature by decreasing the laser power at a constant rate. The maximum cooling rate was approximately 1000°C/s when the laser was turned off at 2000°C. The cooling rate decreased from 1000°C/s to 1°C/s by gradually decreasing the laser power. The crystallization temperature T_X is the temperature at which the temperature starts to increase as crystallization begins. The crystallization time t_X is the time taken from the start of cooling to the beginning of crystallization at T_X (Fig. 1). CCT diagrams were obtained by plotting T_X vs. t_X for various cooling rates. When the melt was not levitated and touched the container wall, the melt always crystallized very quickly with very small undercooling temperature, and the CCT diagram could not be obtained. The solidified phases were identified using Cu $K\alpha$ X-ray diffraction measurements.

3. Rsults

The results of solidification from the levitated melt when the laser power was turned off at 2000°C for the maximum cooling rate are shown in the phase diagram of the SrO–Al_2O_3 system (Fig. 2).[22] Colorless and transparent glasses were obtained in not only the SrO-rich regions[21] but also the Al_2O_3-rich region. The containerless condition is critical for the glass formation. The glass-forming region is divided into two. This might be attributed to the crystalline $SrAl_2O_4$ that exists up to the liquidus line at x = 50 as a stable state. Although compounds with x = 35, 45, 55, and 75 vitrified at a high cooling rate, they crystallized when the cooling rate was low. On the other hand, x = 65 melt did not crystallize within the measured range of the cooling rates, indicating that this composition has higher glass-forming ability than those with x = 35, 45, 55, and 75.

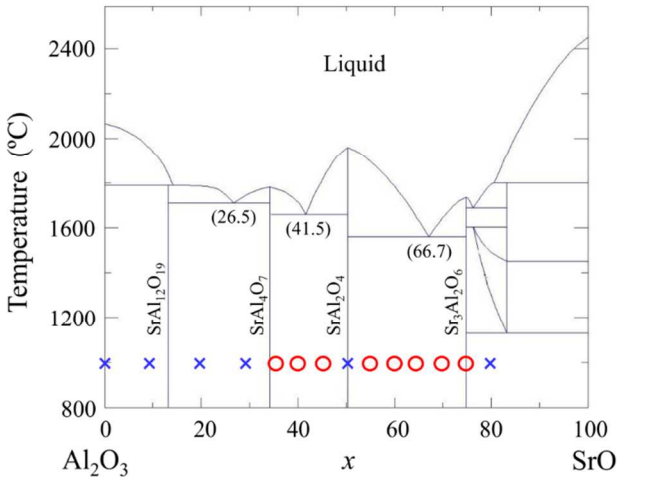

Fig. 2 Solidification from a levitated melt in the SrO–Al_2O_3 binary system after the laser was turned off at 2000°C, corresponding to the maximum cooling rate. Circles and crosses represent glass formation and crystallization, respectively.

Figure 3 shows some cooling curves of xSrO–(100−x)Al_2O_3 (x = 0, 35, 45, 50, 55, and 75). The temperature often oscillated when the sample shape was ellipsoidal and the sample was rotated. This is because of the thermal gradient in the levitated melt between the top side where the laser is applied and the bottom side where the gas flows.[14,18] In the solidification of the

x = 35 melt, there was no detectable temperature rise when the cooling rate was higher than 100°C/s and the sample fully vitrified (Fig. 3 inset). There are five cooling curves with corresponding rates of 72°C/s, 17.4°C/s, 5.6°C/s, 4.2°C/s, and 1.5°C/s. When the cooling rate was 17.4°C/s, 5.6°C/s, 4.2°C/s, or 1.5°C/s, the temperature after recalescence agrees with the melting point, and the solidified samples were fully crystallized. However, when the cooling rate was 72°C/s, the temperature after recalescence did not reach the melting point. The solidified samples were mixtures of crystals and glass (Fig. 3 inset). When the spot of the pyrometer was at a glass region and a crystallized region, the measured temperature was the average of both regions. Thus, the measured temperature does not reach the melting point although the temperature of the crystallized region reached the melting point because the temperature of the glass region decreases. Furthermore, the crystallization temperature T_X was almost the same when the solidified sample was fully crystallized, whereas it was clearly lower for the cooling rate of 72°C/s. This phenomenon was also reported in the cooling curves of the metallic glasses in an ADL furnace.[17] For x = 45, 55, and 75 compounds, a similar behavior was observed. Compounds with x = 0 and 50 were fully crystallized even at the maximum cooling rate, and the temperature after recalescence always reached the melting point. T_X of x = 50 decreased with an increasing cooling rate; however, T_X of x = 0 did not show a clear decrease.

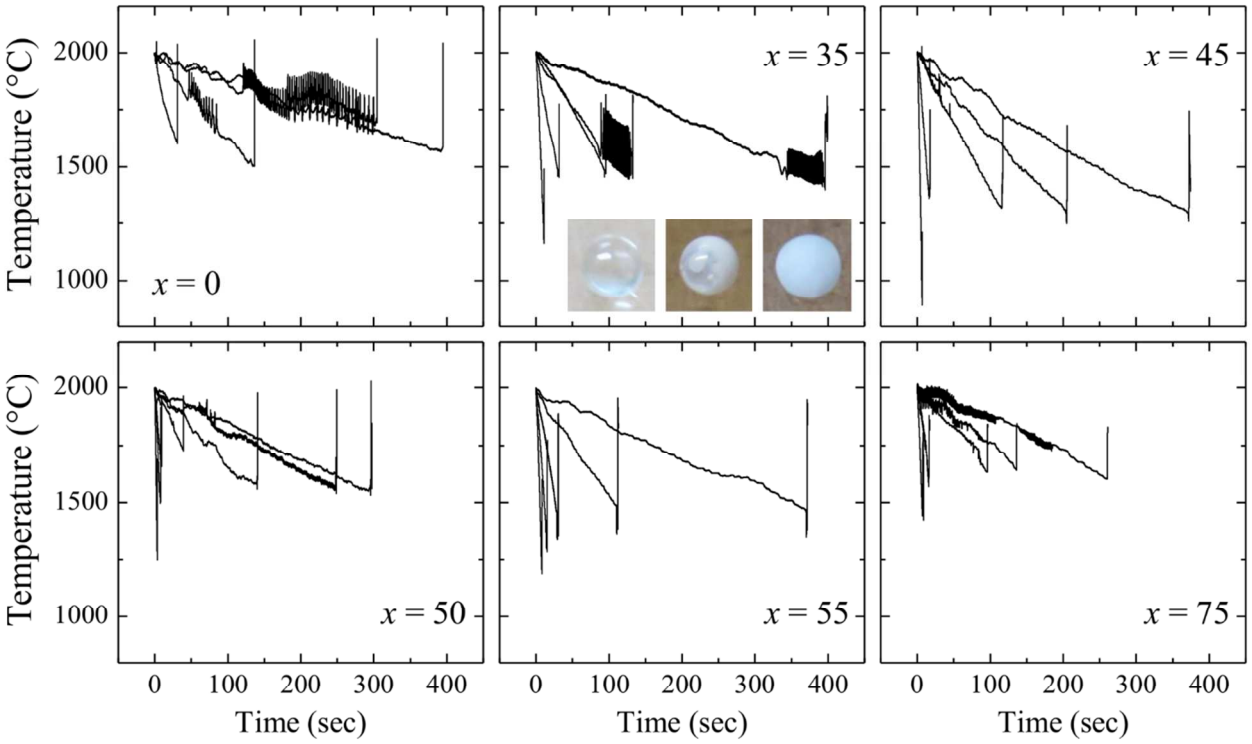

Fig. 3 Cooling curves of xSrO–(100–x)Al_2O_3 (x = 0, 35, 45, 50, 55, and 75). The insets in the graph of x = 35 show glass, partially crystallized glass, and fully crystallized sample.

Figure 4 shows the CCT diagrams of xSrO–(100−x)Al_2O_3 (x = 0, 35, 45, 50, 55, and 75), where T_X vs. t_X is plotted. The dark gray area denotes cooling rates higher than the maximum cooling rate. The light gray area represents the area of colorless and transparent glass. The closed triangles denote that the temperature after recalescence returned to the melting point and the samples were fully crystallized. The open circles indicate that the temperature did not reach the melting point, and the solidified samples were mixtures of glass and crystals. In the CCT diagram of compound with x = 55, it is evident that T_X is almost constant for a slow cooling rate and gradually decreases with an increasing cooling rate. Furthermore, for T_X lower than this constant value, the solidified samples are not fully crystallized. A similar behavior was observed in the case of x = 35, 45, and 75 compounds. The decrease in T_X at a high cooling rate might be a sign of glass formation. In the case of x = 50, constant T_X at a low cooling rate was also observed. However, although T_X decreased at a high cooling rate, the solidified sample was still fully crystallized. A little higher cooling rate may be sufficient for glass formation at x = 50. By contrast, in the case of x = 0, T_X does not decrease at a high cooling rate. This indicates that the x = 0 compound is more difficult to vitrify than x = 50. The R_C for obtaining amorphous Al_2O_3 is over 10^5°C/s;[16] hence, 50SrO–50Al_2O_3 glass would be obtained at cooling rates lower than 10^5°C/s.

Using the CCT diagram, the glass-forming ability of these compounds is quantitatively evaluated. Experimentally, glasses

were easily obtained for compositions in the following order: x = 65, x = 45 and 55, and x = 35 and 75. R_C was calculated from the equation $R_C = (2000-T_n)/t_n$, where T_n is the crystallization temperature at the shortest time t_n. R_C is 100°C/s for x = 35, 110°C/s for x = 45, 140°C/s for x = 55, and 170°C/s for x = 75. All R_C are approximately in the order of 10^2°C/s. R_C does not change significantly and does not seem to correlate with the ease in glass formation. A small difference in R_C in the SrO–Al_2O_3 system is not appropriate to evaluate the glass-forming ability, because R_C is a good measure of the glass-forming ability when R_C is different by several orders of magnitude. The temperature difference (ΔT) between the melting point and the crystallization temperature of the samples can also be extracted from the CCT diagrams. ΔT is 298°C for x = 35, 503°C for x = 45, 491°C for x = 55, and 176°C for x = 75. These values correspond to the order of the glass-forming ability. Therefore, ΔT may be a good measure of the glass-forming ability for compositions at the edge of the glass-forming region.

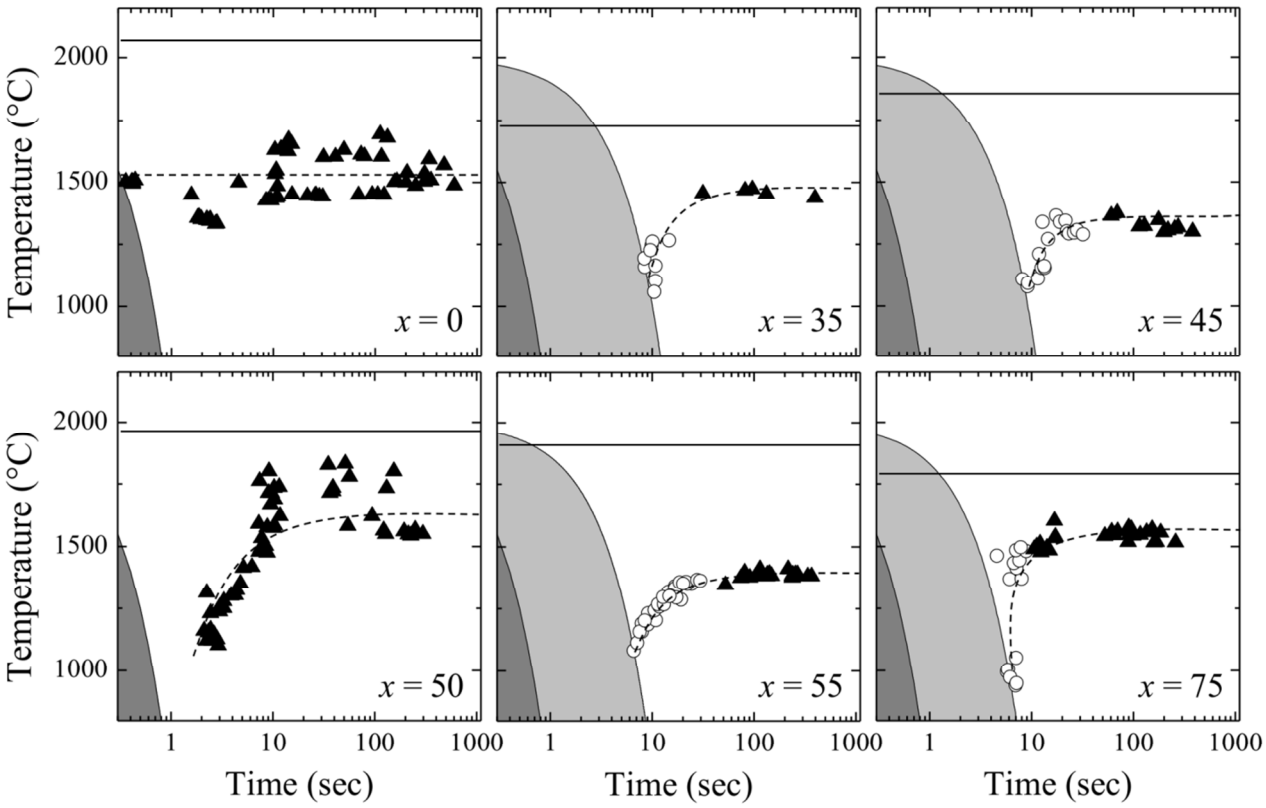

Fig. 4 CCT diagrams of xSrO–(100–x)Al_2O_3 (x = 0, 35, 45, 50, 55, and 75). Data for t_x and T_x (symbols) are derived from the cooling curves. Filled triangles represent the fully crystallized solid sample, while open circles represent the partially crystallized solid sample. The dark gray area is the region where the cooling rate is too fast in our experimental setup. The light gray area indicates the cooling rates for which the solidified samples are fully vitrified. The solid lines indicate the melting point and the dotted lines are for visual aid.

4. Discussion

Generally, in an experimentally obtained CCT diagram, T_X increases with decreasing cooling rates and approaches the melting point, and the CCT curve appears as a half C. When the cooling rate is very low, crystallization always starts at a lower degree of undercooling because heterogeneous nucleation dominates crystallization. The increase in T_X is also observed in theoretically calculated CCT diagrams, although heterogeneous nucleation is not considered.[1,3,4] In the case of the homogeneous nucleation theory, the volume fraction of the crystals at time t is represented by the product of the crystal growth rate U, the nucleation frequency I_υ, and t.[1,3,4] The crystal growth rate U and homogeneous nucleation frequency I_υ are as follows.[3]

$$U = f\nu a_0 \left\{1-\exp\left(-\Delta H_f^m \Delta T_r / RT\right)\right\} \quad (1)$$

$$I_\upsilon = N_\upsilon^0 \nu \exp\left(\frac{-1.024}{T_r^3 \Delta T_r^2}\right) \quad (2)$$

The fraction of sites at the crystal–liquid interface where atoms may be preferentially added or removed is denoted as f, ΔH_f^m is the molar enthalpy of fusion, ΔT_r is the reduced undercooling $(T_m-T)/T_m$ (T_m is the melting point), N_υ^0 is the mean volume concentration of atoms, and T_r is the reduced temperature T/T_m. The frequency of transport ν at the nucleus–liquid and crystal–

liquid interfaces can be related to the liquid viscosity η through the Stokes–Einstein coefficient $\nu = kT/3\pi a_0{}^3\eta$, where k is the Boltzmann constant and a_0 is the atomic diameter. Some of the parameters of SrO–Al_2O_3 binary liquids in the equations, such as the temperature dependence of viscosity, however, are difficult to obtain experimentally now because of their high temperature melting points.

With increasing undercooling or decreasing temperature from T_m, U increases just below T_m and then decreases at a lower temperature. I_υ shows a similar behavior but the increase in I_υ starts far below T_m. When the curves of I_υ and U do not overlap at any temperature, crystallization cannot occur, and the melt will easily transform to glass. For model materials typically considered in the homogeneous nucleation theory, both curves overlap at a range of temperature between the lowest temperature of U, $T_{U,\mathrm{low}}$ and the highest temperature of I_υ, $T_{I\upsilon,\mathrm{high}}$. Crystallization will proceed when the temperature of the undercooled melt is in the overlapping temperature region. With increasing temperature above $T_{U,\mathrm{low}}$, I_υ decreases, whereas U increases. In this case, crystallization will start at a later time with increasing temperature. Therefore, the CCT curve is of the C type with gradually increasing t_x and T_X, as shown in Fig. 5(a). However, because crystallization cannot occur above $T_{I\upsilon,\mathrm{high}}$, the CCT curve does not approach the melting point.

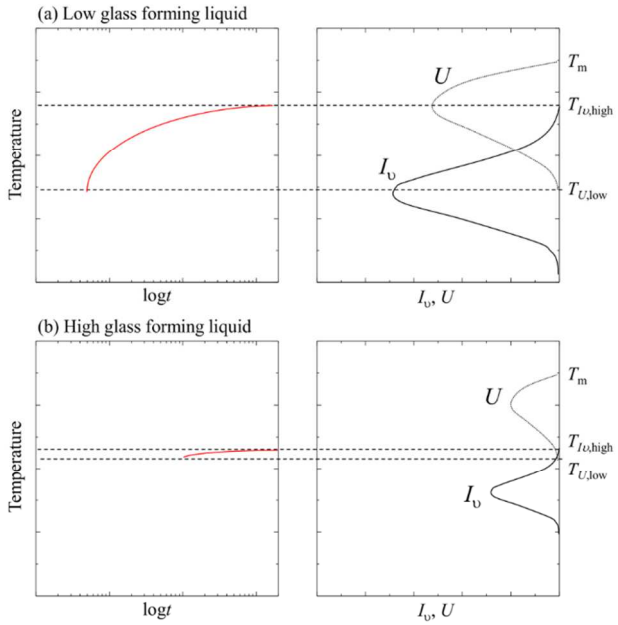

FIG. 5. Schematic of the CCT (left side) and crystallization diagrams from an undercooled melt (right side) of (a) a low glass-forming liquid and (b) high glass-forming liquid. $T_{I\upsilon,\mathrm{high}}$ and $T_{U,\mathrm{low}}$ represent the highest temperature of I_υ and the lowest temperature of U, respectively. T_m is the melting point.

Considering that containerless processing suppresses heterogeneous nucleation, crystallization under containerless conditions should be primarily dominated by homogeneous nucleation, as shown theoretically. In our experiments, however, T_X apparently approached constant values far below the melting point and did not change significantly at low cooling rates. The apparent time-independent feature of T_X was also seen in previous containerless experiments.[17] The characteristic features are discussed below. First, the typical case of the theoretical model is based on the premise that crystallization tends to occur. Conversely, SrO–Al_2O_3 binary liquids have higher glass-forming ability than theoretical models. Therefore, we infer that the overlapping region of the temperatures of U and I_υ is narrower and the values of U and I_υ are smaller, as shown in Fig. 5(b). In this case, even just above $T_{U,\mathrm{low}}$, I_υ has no large values. Thus, crystallization occurs but requires longer time than the theoretical model because of the small I_υ. With increasing temperature, I_υ decreases to zero, and the increase in U is not large compared with the theoretical model. Accordingly, the increase in T_X is strongly suppressed. Therefore, the CCT curves are of the C type but apparently maintain the constant temperatures far below the melting point and do not change significantly at low cooling rates. The characteristic feature of the CCT curves in our experiments could be explained by considering the glass-forming ability at the edge of glass-forming region. The containerless solidification results of the SrO–Al_2O_3 binary system provide a unified model for compounds with a wide range of glass-forming ability. For further quantitative study to evaluate crystallization process under containerless condition, the parameters in the equation (1) and (2) will be obtained in the future experiments.

5. Conclusions

Using an ADL furnace, we determined the glass-forming regions in the SrO–Al_2O_3 system at 35–45 mol% SrO and 55–75 mol% SrO. Cooling curves were obtained at a constant cooling rate in the range 1–1000°C/s. The crystallization temperature was apparently independent of the cooling rate and far below the melting point when the sample was fully crystallized, whereas it decreased when the sample was not fully crystallized. The glass-forming ability can be evaluated quantitatively using the difference between the crystallization temperature and melting point under containerless conditions. Even in the case of fully crystallized compositions, the glass-forming ability can be compared by analyzing the shape of the CCT curve at x = 0 and 50. Furthermore, the apparent time-independent feature of the crystallization temperature is attributed to the high glass-forming ability of the SrO–Al_2O_3 system compared with theoretical calculations. The results suggest that the experimentally obtained CCT diagrams under containerless conditions provide new insights regarding solidification from an undercooled melt.

Acknowledgements

This study was supported in part by Grant-in-Aid for Young Scientists (B) (19750174 and 23750236) and Grant-in-Aid for Scientific Research (C) (21550185 and 25410236) from the Ministry of Education, Culture, Sports and Science and Technology of Japan.

Notes and references

Institute of Industrial Science, The University of Tokyo, 4-6-1 Komaba, Meguro-ku, Tokyo 153-8505, Japan. E-mail: masuno@iis.u-tokyo.ac.jp; Tel: +81-3-5452-6317; FAX: +81-3-5452-6316

REFERENCES

1 D. R. Uhlmann, *J. Non-Cryst. Solids*, 1972, **7**, 337–348.
2 C. G. Levi, V. Jayaram, J. J. Valencia, and R. Mehrabian, *J. Mat. Res.*, **1988**, 5, 969–983.
3 H. A. Davies, *J. Non-Cryst. Solids*, 1975, **17**, 266–272.
4 P. I. K. Onorato and D. R. Uhlmann, *J. Non-Cryst. Solids*, 1976, **22**, 367–378.
5 P. R. Anderson, III, J. Steinberg, and A. E. Lord, Jr., *J. Non-Cryst. Solids*, 1979, **34**, 267–272.
6 H. H. Hng, Y. Li, S. C. Ng, and C. K. Ong, J. Non-Cryst. Solids, 1996, **208**, 127–138.
7 K. Morinaga and H. Takebe, Ber. Bunsenges. Phys. Chemie, 1996, **100**, 1423–1427.
8 K. Nakashima, K. Noda, and K. Mori, J. Am. Ceram. Soc., 1997, **80**, 1101–1110.
9 N. Nishiyama and A. Inoue, Mater. Trans., 1997, **38**, 464–472.
10 X. H. Lin, W. L. Johnson, and W. K. Rhim, Mater. Trans., 1997, **38**, 473–477.
11 C. C. Hays, J. Schroeres, W. L. Johnson, T. J. Rathz, R. W. Hyers, J. R. Rogers, and M. B. Robinson, Appl. Phys. Lett., 2001, **79**, 1605–1607.
12 S. -B Lee, S. -K Lee, and N. J. Kim, Mater. Trans., 2007, **48**, 1501–1504.
13 S. S. Jung and I. Sohn, J. Am. Ceram. Soc., 2013, **96**, 1309–1316.
14 J. K. R. Weber, C. D. Anderson, D. R. Merkley, and P. C. Nordine, J. Am. Ceram. Soc., 1995, **78**, 577–582.
15 T. Aoyama, Y. Takamura, and K. Kuribayashi, Metall. Mater. Trans. A, 1999, **30**, 1333–1339.
16 D. M. Herlach, D. Holland-Moritz, Th. Schenk, K. Schneider, G. Wilde, O. Boni, J. Fransaer, and F. Spaepen, J. Non-Cryst. Solids, 1999, **250–252**, 271–276.
17 J. J. Wall, R. Weber, J. Kim, P. K. Liaw, and H. Choo, Mater. Sci. Eng. A, 2007, **445–446,** 219–222.
18 A. C. Barnes, L. B. Skinner, P. S. Salmon, A. Bytchkov, I. Pozdnyakova, T. O. Farmer, and H. E. Fischer, Phys. Rev. Lett., 2009, **103**, 225702.
19 P. C. Nordine, D. Merkley, J. Sickel, S. Finkelman, R. Telle, A. Kaiser, and R. Prieler, Rev. Sci. Instrum., 2012, **83**, 125107.
20 D. Herlach, P. Galenko, and D. H. Moritz. Metastable Solids from Undercooled Melts Elsevier (2007).
21 M. Licheron, V. Montouillout, F. Millot, and D. R. Neuville, J. Non-Cryst. Solids, 2011, **357**, 2796–2801.
22 ACerS–NIST Phase Equilibria Diagram CD-ROM Database Version 3.2.

The continuous cooling transformation (CCT) diagrams of the $SrO–Al_2O_3$ binary system under containerless condition using an aerodynamic levitation furnace provide the slight difference in glass-forming ability at the edge of the glass-forming region.

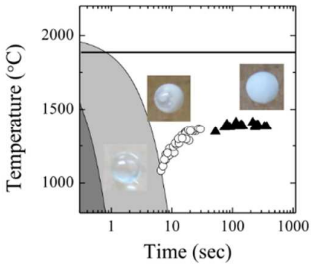

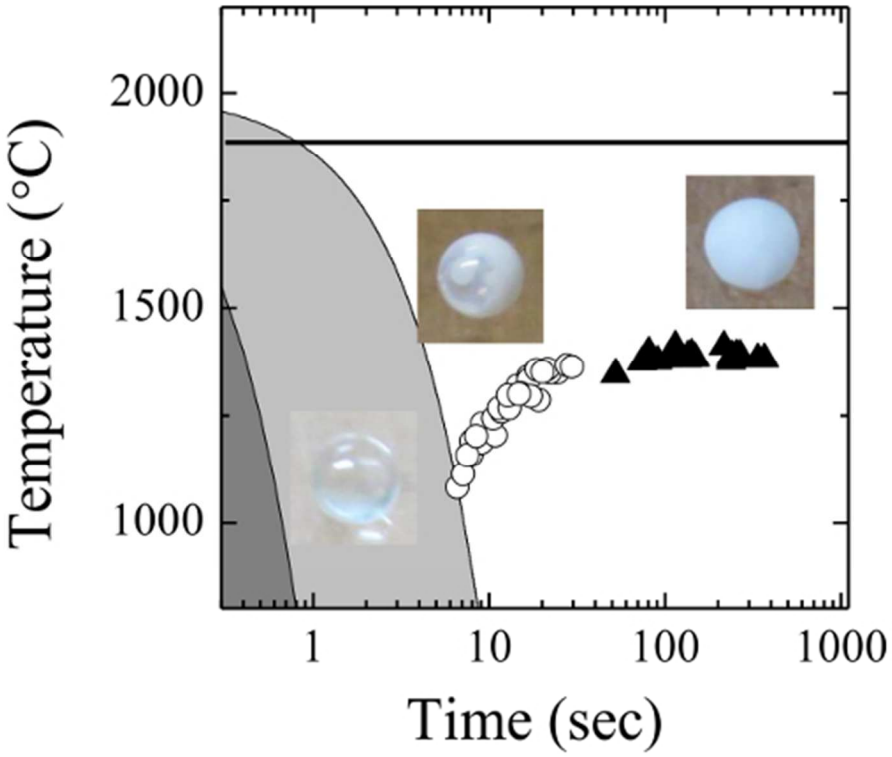

48x39mm (300 x 300 DPI)